

Article

Design of Tri-Band Patch Antenna with Enhanced Bandwidth and Diversity Pattern for Indoor Wireless Communication

Min Gao ^{1,2}  and Xiaohu Zhao ^{2,3,*}

¹ School of Mechanical and Electrical Engineering, Hefei Technology College, Hefei 230601, China; mghfhtc@126.com

² School of Information and Control Engineering, China University of Mining and Technology, Xuzhou 221000, China

³ The National Joint Engineering Laboratory of Internet Applied Technology of Mines, Xuzhou 221000, China

* Correspondence: zhaoxiaohu@cumt.edu.cn

Abstract: A novel tri-band patch antenna with enhanced bandwidth and a diverse radiation pattern is presented in this study. An off-center probe is introduced to excite a conventional circular patch antenna, and the multi-frequency resonance modes of TM_{01} , TM_{02} , and TM_{03} with different radiation properties are obtained. Four metal cambered strips are distributed around the circular patch to adjust the impedance matching of the circular patch antenna. In order to widen the impedance bandwidth, a parasitic patch placed above the circular patch antenna is employed in this work. Then, a double-layer patch antenna is manufactured and tested to verify the accuracy of the theoretical analysis and simulated result. The measured results, which are basically consistent with the simulated results, show that the designed antenna can operate in three bandwidths of 1.79–1.81 GHz, 3.74–4.0 GHz, and 4.93–5.44 GHz, with radiation patterns of directional, omnidirectional, and three-beam pointing. The radiation efficiency higher than 85.6% and the maximum gain greater than 9.42 dBi suggest that the investigated antenna is suitable for multi-service scenarios in wireless communication.



Citation: Gao, M.; Zhao, X. Design of Tri-Band Patch Antenna with Enhanced Bandwidth and Diversity Pattern for Indoor Wireless Communication. *Appl. Sci.* **2022**, *12*, 7445. <https://doi.org/10.3390/app12157445>

Academic Editor: Wei Gong

Received: 20 June 2022

Accepted: 18 July 2022

Published: 25 July 2022

Publisher's Note: MDPI stays neutral with regard to jurisdictional claims in published maps and institutional affiliations.



Copyright: © 2022 by the authors. Licensee MDPI, Basel, Switzerland. This article is an open access article distributed under the terms and conditions of the Creative Commons Attribution (CC BY) license (<https://creativecommons.org/licenses/by/4.0/>).

Keywords: patch antenna; enhanced bandwidth; diverse radiation pattern; multi-frequency resonance mode; multi-service; wireless communication

1. Introduction

With the continuous emergence of various wireless services and new scenarios, more and more wireless communication systems will coexist for a long time, with increasing requirements for the miniaturization, intelligence, and multi-function of wireless communication systems. A multi-band antenna with pattern diversity can not only support the working frequency bands under multiple wireless system standards, but can also meet the specific needs of the communication system for polarization and radiation direction in different frequency bands, greatly increasing the functionality of the antenna. However, the structure of the antenna with related functions is relatively complicated, and the radiation performance also needs to be improved.

In [1], a center-fed circular patch antenna with a monopole-like radiation pattern is proposed. A group of metal vias concentrically surrounds the circular patch and shorted ground plane. Attributed to the shorted vias, the TM_{01} and TM_{02} modes are excited, and the measured results show that an impedance bandwidth of 18% with a maximum gain of 6 dBi is achieved. Combined with the center-fed circular patch and shorted metal via technology, two dual-band stacked patch antennas are designed in [2,3]. In [2], a stacked-patch structure is constructed to generate a weak coupling effect; then, dual-band performance with an omnidirectional pattern is acquired. A truncated patch etched with a U-shaped slot is placed on the upper layer of the antenna in [3] to achieve a unidirectional radiation pattern with circular polarization characteristics. Meanwhile, an omnidirectional radiation pattern with the feature of linear polarization is obtained by introducing TM_{01} and

TM₀₂ modes generated by a lower circular patch. Antennas that have a stacked structure are also proposed in [4,5]. In [4], an artificial magnetic conductor (AMC) characterized by four zero-phases of reflection coefficient is placed on a quad-band coplanar waveguide (CPW) antenna to achieve multi-band and high gain characteristics. Unlike [4], Ref. [5] adopts a dual-antenna design technique. The upper and lower layers of the antenna are, respectively, a printed dipole array responsible for horizontal polarization and a discone antenna responsible for vertical polarization. The measured results show that the two polarization modes of the antenna can work in two bandwidths of 770–980 MHz and 1.69–3.21 GHz, respectively.

In [6,7], two dual-band patch antennas with radiation-differentiated characteristics are presented by employing different radiating elements. However, the maximum gain of these two antennas at the lower band is only 3.1 dBi. Based on multi-resonant modes, two dual-band, dual-polarized antennas are investigated in [8,9]. However, the impedance bandwidths of the designed antennas are lower than 3.6%. In [10], a rectangular patch loading a branch on one radiating side and etching a rectangular slot on the other side is proposed to generate TM₀₁ mode and modified TM₂₀ and TM₃₀ modes. The measured result shows that the single patch antenna can operate at three bands and the measured patterns are characterized by broadside radiation. A similar method is also applied in [11] to introduce three sets of orthogonal modes, and then three resonance bandwidths with circular polarization characteristics are obtained. In [12], a novel multi-band patch antenna with unidirectional radiation is designed, based on a coupled resonators network. The four frequency bands can be adjusted by changing the coupling strength between the resonators. In addition, the operation bands can be adjusted without changing the shape of the antenna, providing a flexible method of antenna design. However, the measured bandwidths of the antennas in [10–12] are relatively narrow. By loading two types of slots on the patch antenna, the method of obtaining multi-resonant modes for the antenna and increasing the bandwidth of the antenna is applied in [13]. A composite right/left-handed transmission line technique is also introduced to design the patch antenna with the feature of multi-frequency in [14]. Compared with the technologies of the shorted via, slotting, and stacked structure, the composite right/left-handed transmission line can not only increase the resonant band, but also has the advantages of reducing cross-polarization and enhanced gain, as shown in [15,16]. However, for the antennas in [14–16], the characteristics of miniaturization, low profile, multi-band, and high gain are not concentrated in a particular antenna.

In this study, a patch antenna with the characteristics of tri-band, enhanced bandwidth, high gain, and a diverse radiation pattern is investigated. Two circular substrates are placed up and down to form a double-layer structure. A circular patch printed on the upper surface of Substrate 1 is directly excited by an off-center probe. Meanwhile, four metal cambered strips surround the outer side of the circular patch to adjust the impedance matching. Then, TM₀₁, TM₀₂, and TM₀₃ resonance modes with acceptable reflection coefficients are obtained. Furthermore, a parasitic patch located on the upper surface of Substrate 2 widens the impedance bandwidth of the patch antenna by coupling with the circular patch. The measured results show that the double-layer patch antenna has differentiated radiation patterns in three frequency bands, with impedance bandwidths of 1.1%, 6.7%, and 9.8%. Moreover, the advantages of the single-probe back-feeding method, simple structure, and easy processing all indicate that the antenna is suitable for multi-service applications.

2. Antenna Design and Theoretical Analysis

As shown in Figure 1, the geometric diagram of the proposed tri-band patch antenna and the optimal size of the corresponding configuration are given. It can be seen that the antenna is composed of two circular substrates and an air layer with a height of H_2 . Substrate 1, which has a permittivity of 2.2, a tangent loss of 0.0001, and a height of H_1 , is located in the lower layer of the antenna. A circular patch with a radius of R_4 and a ground plane with a radius of R_1 are both concentric with Substrate 1, and are printed on

the upper and lower surfaces of Substrate 1. An off-center probe is introduced to change the surface current on the circular patch, which is similar to the principle of etching a slot on the patch [10]. Meanwhile, four cambered strips surrounding the outer side of the circular patch are also printed on the upper surface of Substrate 1. Substrate 2, which has the same electrical parameters as Substrate 1, is located at the uppermost layer of the proposed antenna, but the thickness is selected as $H3$ to reduce the profile height of the overall antenna. A parasitic patch with a radius of $R5$ is printed on the upper surface of Substrate 2. The parasitic patch is excited by the coupling effect with the lower circular patch. Finally, the two substrates and a foam board with a thickness of 0.5 mm in the middle are fixed together with two nylon screws.

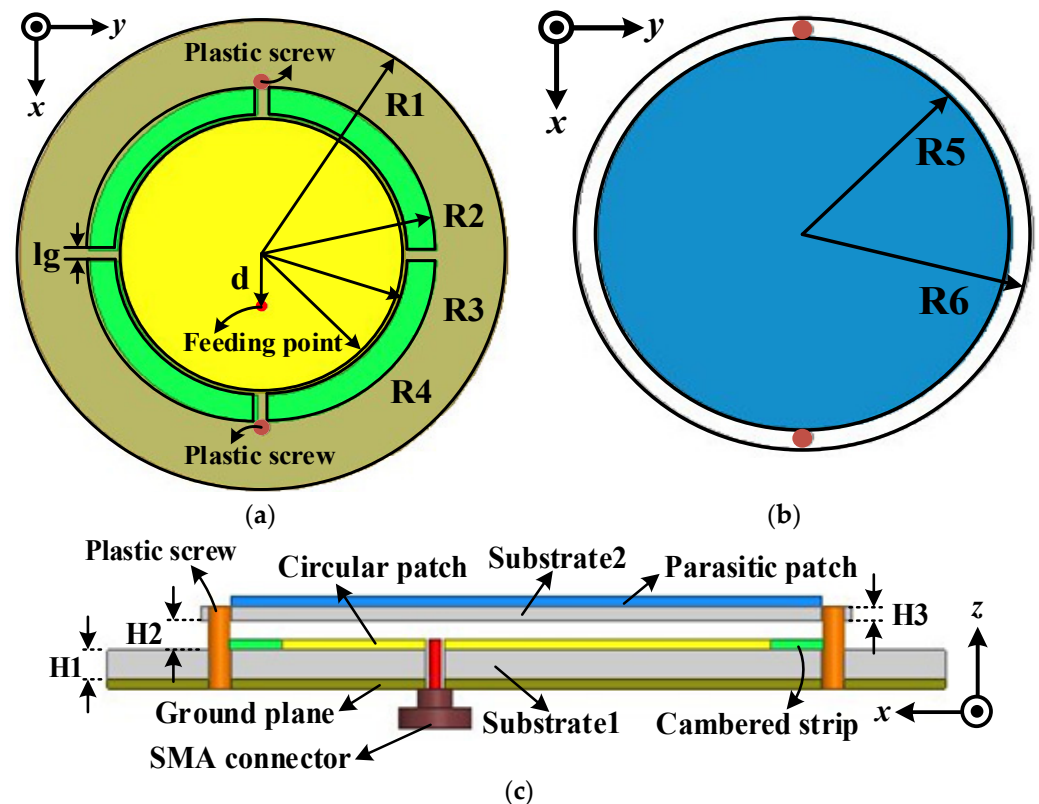


Figure 1. Geometry of the proposed patch antenna: (a) top view of Substrate 1; (b) top view of Substrate 2; (c) side view of the proposed antenna. $R1 = 48$, $R2 = 32$, $R3 = 27$, $R4 = 26.25$, $R5 = 33$, $R6 = 38$, $d = 9.8$, $l_g = 4$, $H1 = 1.5$, $H2 = 0.5$, $H3 = 1.1$ (all dimensions in mm).

In order to clearly explain the working mechanism of the designed antenna for multi-frequency, widened bandwidth, and diverse radiation patterns, the three antennas that appear in sequence during the antenna design process are shown in Figure 2. Ant. 1 is a traditional single-layer circular patch antenna with an off-center probe. Compared with the center-fed circular patch antenna in [1,2,6], the off-center feeding proposed in this paper introduces more resonance modes. As for Ant. 1, the distance between the feeding point and the center of the circular patch is set to d , and the radius of the circular patch is set to $R4$. In terms of the reflection coefficient, a detailed parameter analysis is carried out for these two parameters, and the corresponding simulated results are shown in Figure 3. It can be observed from Figure 3a that when $d = 0$ —that is, when the center-fed probe is employed—the antenna has only one resonance point at 4.53 GHz. As d gradually increases, Ant. 1 exhibits the characteristics of multi-frequency resonance. In detail, when $d = 9.8$ mm, Ant. 1 exhibits a reflection coefficient of less than -10 dB at 2.18 GHz, 3.62 GHz, and 4.48 GHz, respectively. On the basis that d is determined to be 9.8 mm, we further study the influence of $R4$ on antenna resonance. It can be seen from Figure 3b that, as the size of

the circular patch continues to increase, the three resonant frequency points of Ant. 1 all move to lower frequencies. Based on the above discussion, it can be concluded that, for Ant. 1, the position of the feeding point determines the resonance mode of the antenna, and the position of the resonance frequency point is mainly influenced by the size of the circular patch.

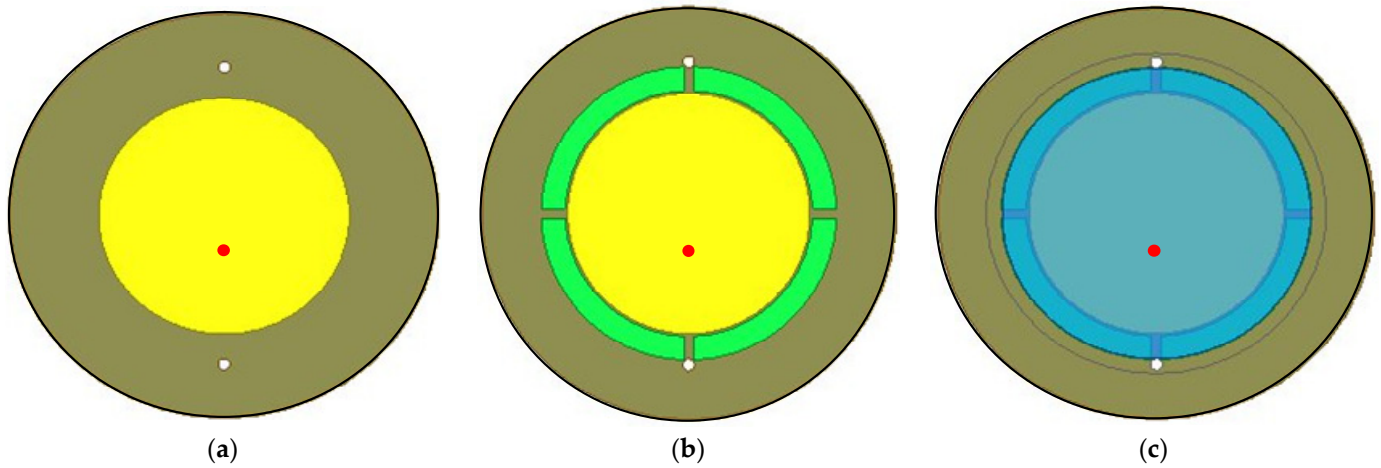


Figure 2. The evolution of the proposed tri-band patch antenna: (a) Ant. 1; (b) Ant. 2; (c) Ant. 3.

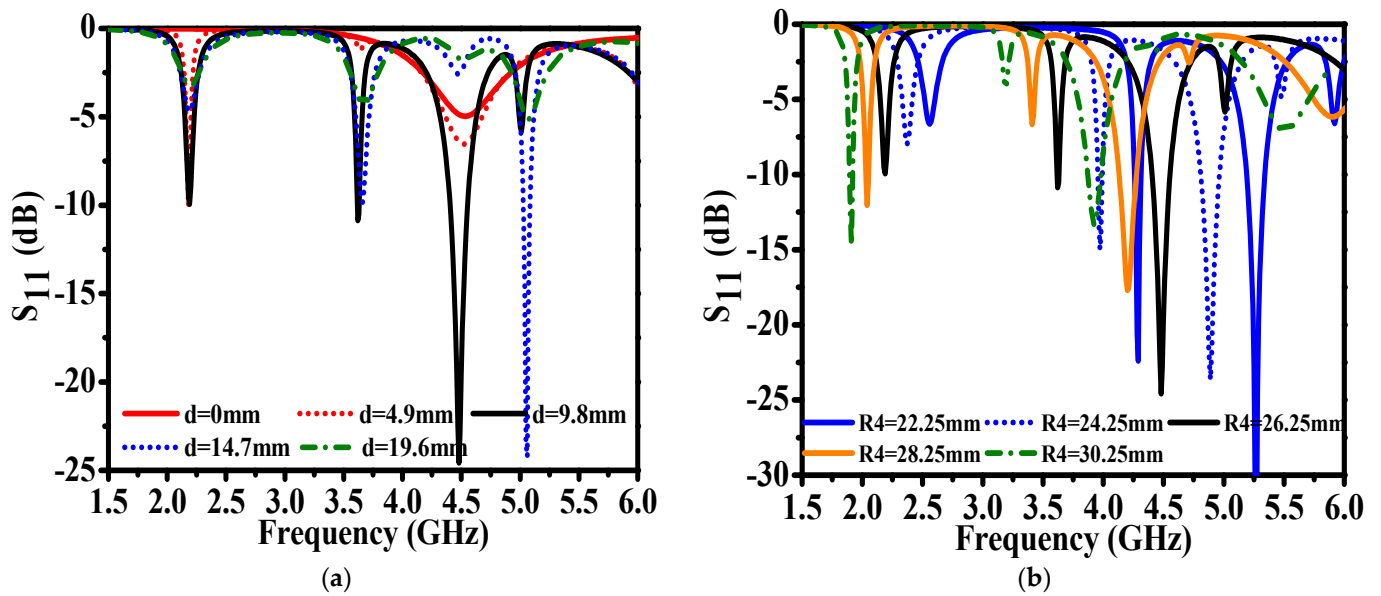


Figure 3. The effect of different parameters on simulated S_{11} of Ant. 1. (a) d ; (b) R_4 .

Since the optimal reflection coefficients of Ant. 1 at the frequency points of 2.18 GHz and 3.62 GHz are greater than -10.56 dB, which fails to meet the requirements of engineering applications, some improvements are implemented in Ant. 1. As shown in Figure 2a, four cambered strips surrounding the outside of the circular patch are introduced to form Ant. 2, and the simulated result of S_{11} is given in Figure 4. It is worth mentioning that metal cambered strips surrounding the circular patch are introduced to improve impedance matching. The specific performance is the gap between the four cambered strips; the gap between the strips and the circular patch is both capacitive and employed to reduce the inductance introduced by the coaxial probe. Compared with the simulated result of Ant. 1, the improved Ant. 2 also has three resonance modes, which are the same as Ant. 1. The specific performance of the reflection coefficient amplitudes of Ant. 2 at the three frequency points of 2.14 GHz, 3.64 GHz, and 4.43 GHz are -15.18 dB, -16.34 dB, and -32.08 dB,

respectively, all of which satisfy the requirement of less than -15 dB. On the basis of Ant. 2, Substrate 2, printed with a parasitic patch, is placed directly above Ant. 2, and an air layer with thickness of 0.5 mm is introduced between the two substrates to form Ant. 3. Attributed to the coupling effect between the circular patch and the parasitic patch, the surface current distribution on the circular patch changes, and the simulated results of S_{11} are given in Figure 4. The simulated results show that the reflection coefficients of Ant. 3 in the three frequency bands of 1.86 – 1.89 GHz, 3.77 – 4.09 GHz, and 5.14 – 5.59 GHz are all lower than -10 dB. According to the location of the frequency band, three resonant frequency bands of Ant. 3 are named f_1 , f_2 , and f_3 (from low to high). Compared with the previous two antennas, Ant. 3 achieves the characteristics of extended bandwidth while maintaining three resonance modes.

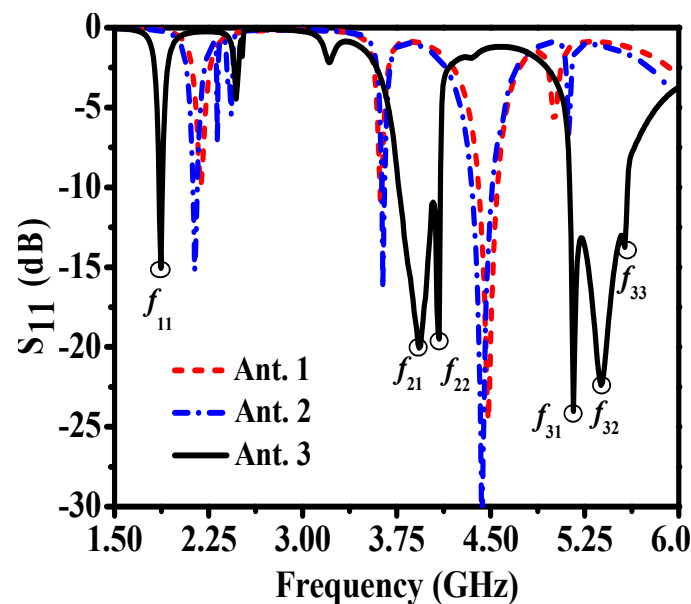


Figure 4. Comparison of simulated S_{11} for the three antennas.

In order to explain the working mechanism of the multi-mode and the expanded bandwidth more clearly, a parameter analysis is carried out for the two key parameters of R_5 and H_2 . The simulated results are shown in Figure 5. As shown in Figure 5a, as the radius R_5 of the parasitic patch increases, f_1 gradually shifts to a lower frequency, accompanied by a gradually deteriorating reflection coefficient. Similarly, f_2 , which has two resonance frequency points, also shows a tendency to move to a low frequency. However, the resonant point f_{22} at the high frequency within f_2 remains basically unchanged, while the resonant point f_{21} at the low frequency gradually moves to an even lower frequency, resulting in the gradual division of f_2 into two adjacent frequency bands. As for the high-frequency band f_3 , Figure 5b shows the detailed simulated results. When the radius R_5 of the parasitic patch is 29.8 mm, Ant. 3 exhibits dual-frequency f_{31} and f_{32} resonance characteristics at 5.24 GHz and 5.72 GHz. When the radius R_5 increases to 31.8 mm in steps of 1 mm, both f_{31} and f_{32} move to a lower frequency, and the distance between the two frequency points gradually decreases. As shown by the solid black line in Figure 5b, adjacent f_{31} and f_{32} form a wide band with an acceptable reflection coefficient, and the additional resonance point f_{33} further extends f_3 . However, as R_5 continues to increase, f_{31} and f_{32} finally merge into the resonance frequency of 5.31 GHz, and the frequency f_{33} is maintained at 5.57 GHz. It is worth noting that the reflection coefficient within f_3 gradually deteriorates as R_5 increases from 31.8 mm to 33.8 mm, and finally, the advantage of broadband is lost.

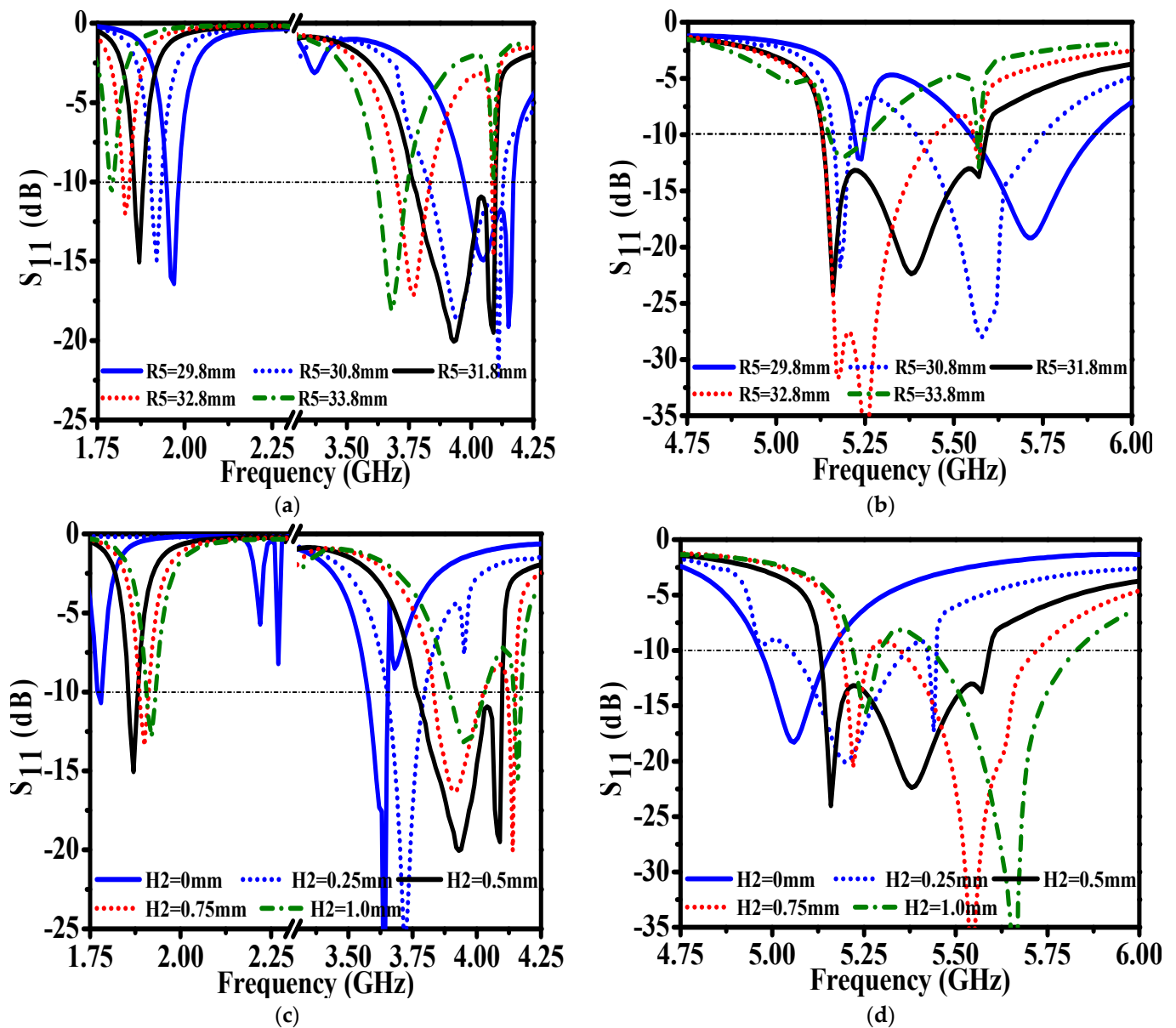


Figure 5. The effect of different parameters on simulated S_{11} of Ant. 3: (a) the effect of different R_5 on frequency bands f_1 and f_2 ; (b) the effect of different R_5 on frequency band f_3 ; (c) the effect of different H_2 on frequency bands f_1 and f_2 ; (d) the effect of different H_2 on frequency band f_3 .

Figure 5c,d show the curve between the reflection coefficient of Ant. 3 and the air-layer thickness H_2 . It can be concluded from Figure 5c that, as H_2 increases, f_1 gradually moves to a higher frequency, and both f_{21} and f_{22} also show a tendency to move to a higher frequency. However, the reflection amplitude of f_{21} gradually increases, and the reflection coefficient of f_{22} exhibits the characteristics of improvement and then deterioration with the increase in H_2 . Figure 5d shows the graph of f_3 varying with H_2 . It can be seen that, when H_2 increases from 0 mm to 0.25 mm, f_3 changes from a single-frequency point resonance of 5.06 GHz to a multi-frequency point resonance. As H_2 continues to increase, f_3 gradually moves to a higher frequency. It can also be observed from [17] that the equivalent permittivity ϵ_{efq} of the substrates with an air layer can be calculated using the following formula:

$$\epsilon_{efq} = \frac{\epsilon_r(H_2 + H_3)}{H_2 \cdot \epsilon_r + H_3} \tag{1}$$

where ϵ_r and $H3$ represent the relative permittivity and thickness of Substrate 2. When the thickness $H2$ of the air layer increases, it can be seen from (1) that ϵ_{eff} gradually decreases, causing the three frequency bands of Ant. 3 to shift to a higher frequency. Finally, 0.5 mm is selected as the optimal value of $H2$ to ensure the broadband characteristics of Ant. 3.

The vector current distribution on the surface of both the circular patch and the parasitic patch is given in Figure 6 to vividly explain the broadband characteristics of Ant. 3. It can be seen from Figure 6a that the current on the parasitic patch at 1.87 GHz mainly flows along the x -axis direction with the characteristics of in-phase. Taking into account the current distribution of the circular patch, it can be concluded that Ant. 3 at 1.87 GHz is working in TM_{01} mode with a broadside radiation pattern. It should be noted that, after the parasitic patch is loaded, the influence of R5 on f_1 is greater than that of R4. Due to the coupling effect between the parasitic patch and the circular patch, the original resonance points of Ant. 2 at 3.64 GHz and 4.43 GHz are close to each other, and finally, f_{21} and f_{22} of Ant. 3 are formed. Figure 6b shows the current distribution on the two patches when Ant. 3 operates at 3.84 GHz. The vector current on the circular patch flows from the center of the patch in two opposite directions along the x -axis, with out-of-phase characteristics. Moreover, the surface current on the parasitic patch also shows out-of-phase flowing from the center of the parasitic patch along the y -axis in two opposite directions. Attributed to the out-of-phase feature, Ant. 3 works at f_2 with an omnidirectional radiation pattern, which is similar to the center-fed monopole patch antenna that resonates in the TM_{02} mode [2]. The benefit of the weak coupling between the circular radiating patch and the parasitic patch, when Ant. 3 works at 5.38 GHz, is that the current distribution of the circular patch is diametrically opposite to that of the parasitic patch, as shown in Figure 6c. Meanwhile, Figure 7a shows the electric field distribution of Ant. 3 at 5.38 GHz, which is the same as the working mechanism of the TM_{03} mode in Figure 7b. Combining Figures 6c and 7, it can be concluded that at 5.38 GHz the TM_{03} mode dominates the working mode of Ant. 3 and the resonance bandwidth is 450 MHz.

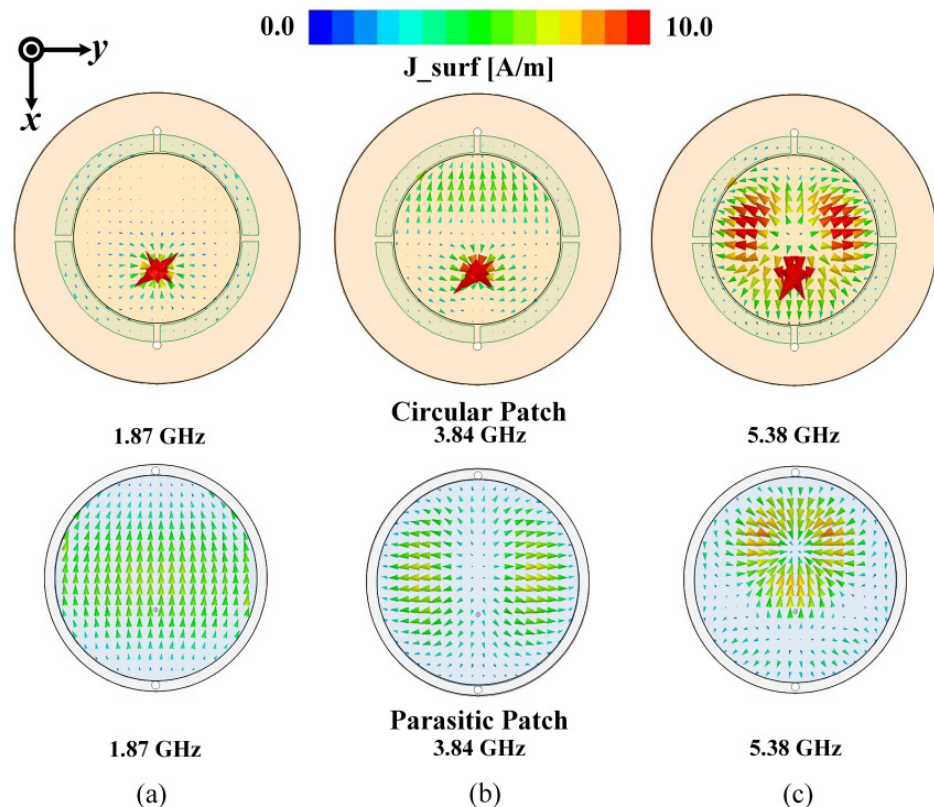


Figure 6. The simulated surface current distribution on the circular patch and parasitic patch of Ant. 3: (a) 1.87 GHz; (b) 3.84 GHz; (c) 5.38 GHz.

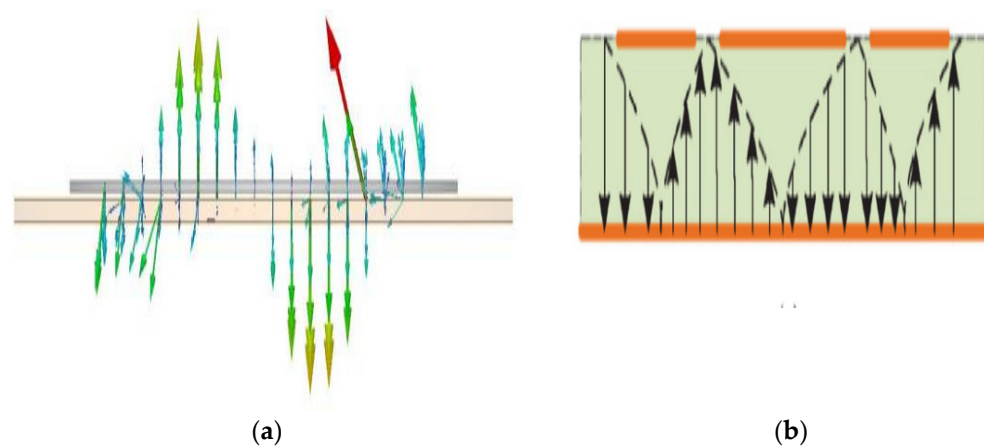


Figure 7. (a) E-field distribution of the Ant. 3 at 5.38 GHz. (b) Sketch of the operation mechanism at TM_{03} mode.

3. Measured Results Discussion

In order to verify the accuracy of the simulated results of Ant. 3, the proposed tri-band patch antenna as shown in Figure 8 is fabricated, and the test items related to reflection coefficient, antenna gain, radiation efficiency, and radiation pattern are also carried out.

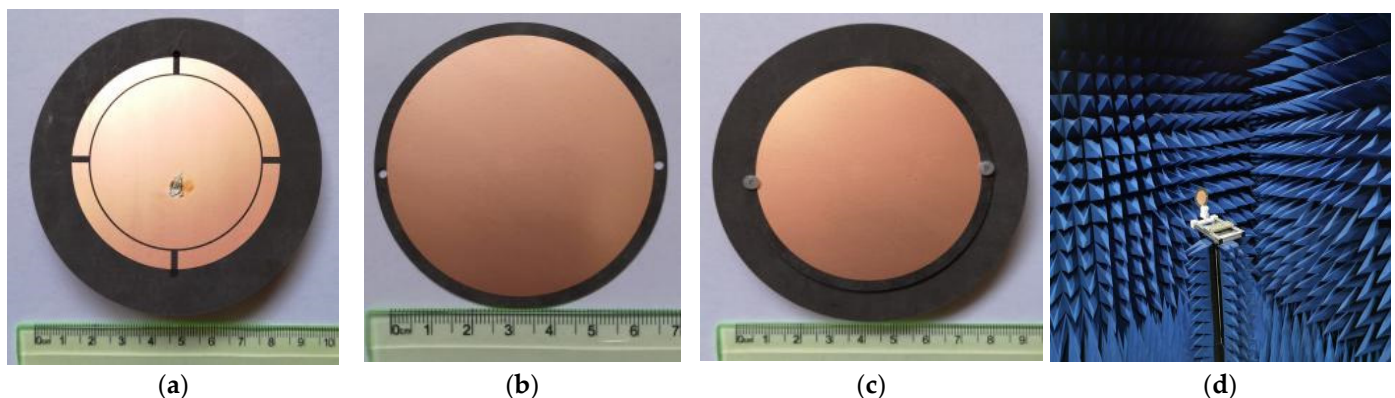


Figure 8. Photography of the fabricated patch antenna: (a) top view of Substrate 1; (b) top view of Substrate 2; (c) top view of the assembled antenna; (d) test process of the fabricated antenna.

Regarding the reflection coefficient of the proposed tri-band patch antenna, the comparison curve between the simulated result and the measured result is depicted in Figure 9. The measured S_{11} shows that the fabricated antenna operates in three frequency bands of f_1 : 1.79–1.81 GHz, f_2 : 3.74–4.0 GHz, and f_3 : 4.93–5.44 GHz. Compared with the simulated results, both f_1 and f_3 show signs of moving towards a lower frequency, which is mainly due to errors introduced during the assembly and testing.

The reasons for the existence of more than three reflection nulls in Ant. 3 can be summarized as follows. Part of the reflection nulls of Ant. 3 is caused by the off-center feeding technology. The benefit of the off-center feeding technology is that Ant. 3 can work in a slot-like mode, which is similar to the principle that etches a slot with a specific shape on the radiating patch to achieve the notch effect. On the other hand, by loading the parasitic patch on the circular radiating patch of the antenna in the corresponding frequency band, the current on the circular patch and the current on the parasitic patch cancel each other out, and a notch response is also introduced.

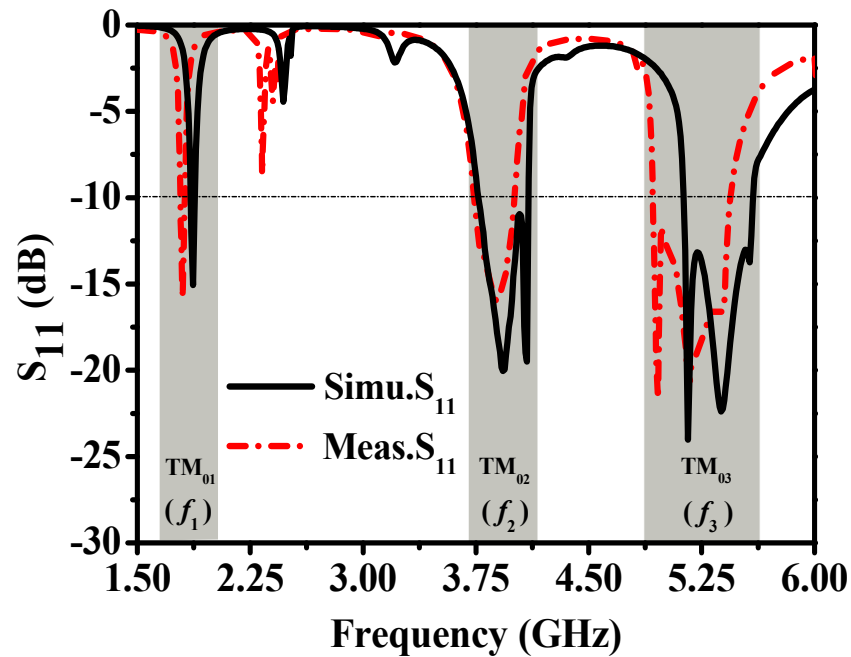


Figure 9. Comparison of simulated results and measured results of the S_{11} .

Meanwhile, Figure 10 shows the measured results of antenna gain and radiation efficiency. As shown in Figure 10a, the measured maximum gains of the antenna in $f_1, f_2,$ and f_3 are, respectively, 6.35 dBi, 6.15 dBi, and 9.42 dBi, which are lower than the simulated gains of 7.20 dBi, 6.74 dBi, and 10.62 dBi. In terms of radiation efficiency, Figure 10 presents the compared results of measurement and simulation. The results show that the measured efficiencies in the three frequency bands are 89.2%, 86.9%, and 85.6%, respectively, and are lower than the simulated results of 98.0%, 93.6%, and 94.7%. The measured antenna gain and radiation efficiency both show partial attenuation, which is mainly due to the loss introduced by the 0.5 mm foam layer and the error in the welding and assembly process.

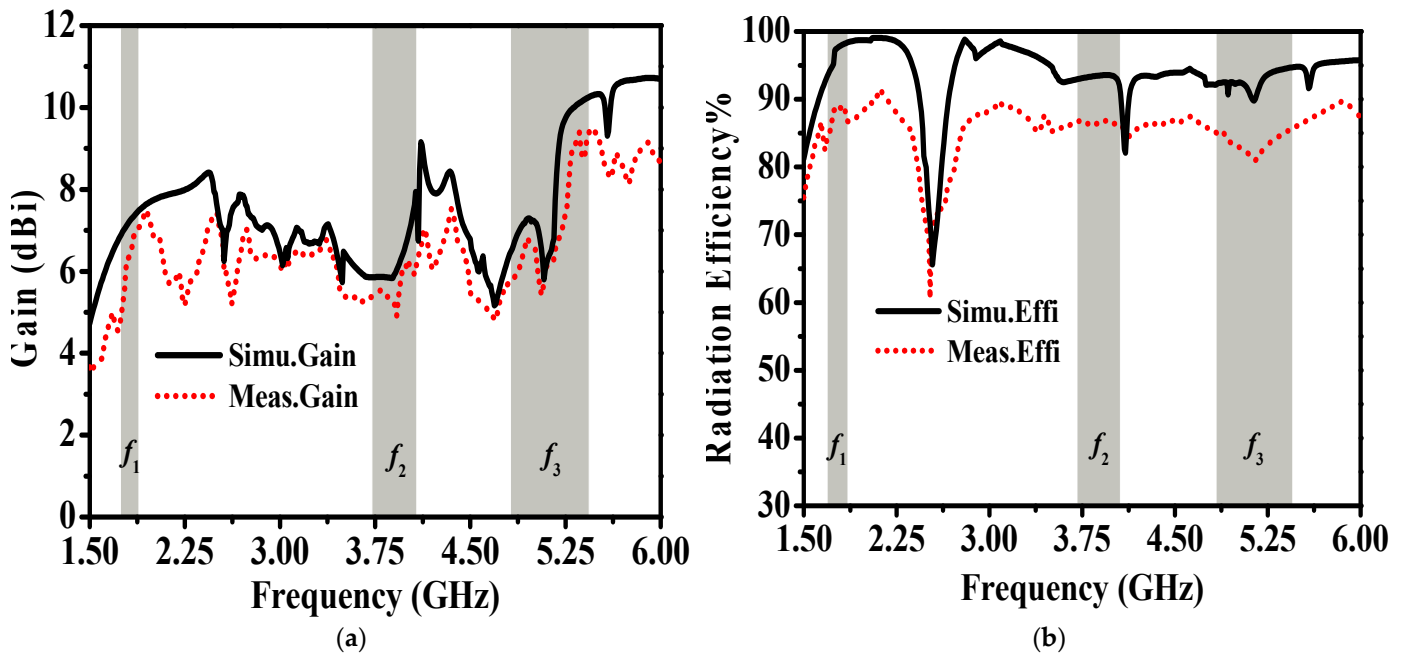


Figure 10. Simulated and measured gains and radiation efficiencies of the designed antenna: (a) gain; (b) radiation efficiency.

In order to visually reveal the pattern diversity of the designed antenna, Figure 11 shows the measured results of the radiation pattern at 1.80 GHz, 3.80 GHz, and 5.35 GHz. As shown in Figure 11a, the patterns which show broadside directional radiation on the xoz and yoZ planes are obtained at 1.80 GHz, while an omnidirectional radiation pattern is achieved on the xoy plane at 3.80 GHz. Figure 11c shows the antenna pattern at 5.80 GHz with the characteristics of three adjacent beams on the xoz plane, which is caused by the introduction of higher-order modes. Based on the above analysis, the proposed Ant. 3 can be utilized for multi-service applications in wireless communication due to the characteristics of multi-mode operation, pattern diversity, and expanded bandwidth.

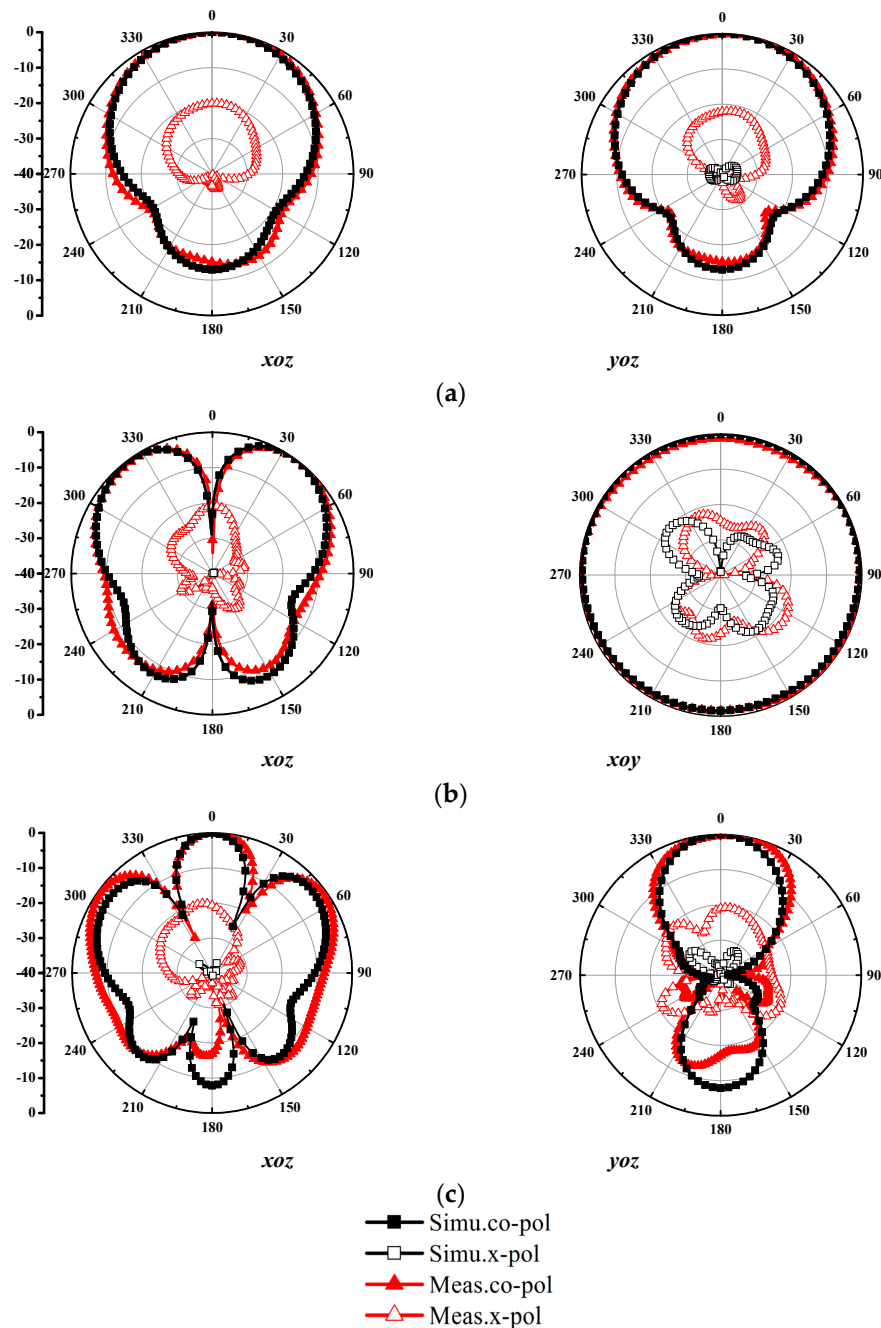


Figure 11. Simulated and measured radiation patterns of the designed antenna in xoy , xoz , and yoZ planes: (a) 1.80 GHz; (b) 3.80 GHz; (c) 5.35 GHz.

4. Comparison

As Table 1 shows, shorted via technology is employed in [1–3] to achieve the features of multi-band and broadband. Although the bandwidths of these antennas are all greater than 9%, the cross-polarization ratio below 18 dB and the size exceeding $1.3\lambda_0$ are not conducive to antenna integration and miniaturization applications. Slotting, shorted vias, and resonant stubs have been used in cross-combination to achieve multi-frequency characteristics. For example, in [10,11], additional resonant modes are introduced by etching slots on the radiating patch and loading parasitic resonant branches. In [18], a miniaturized antenna with four operating bandwidths is designed by combining slotting and shorted vias techniques. However, the gain of the antenna of below 2.5 dBi and the low radiation efficiency are problems that need to be solved. A defected ground structure and coupled resonator network are also investigated in [4,12], respectively, obtaining tri-band and quadband resonance characteristics. For these two multi-band antennas, the advantages of broadband and high gain can only be realized as separate advantages on the individual antennas.

Table 1. Comparison Between Reported and the Proposed Antenna.

Ref.	IMBW (%)	PG (dBi)	Effi (%)	XPR (dB)	Size (λ_0^3)	Num. of Band	Ways to Achieve Multi-Band and Wideband
[1]	18	6	-	≥ 15	$1.35 \times 1.35 \times 0.02$	1	Shorted vias
[2]	12.2 & 9.8	6 & 7.5	≥ 80	≥ 18	$1.35 \times 1.35 \times 0.03$	2	Stacked patch & shorted vias
[3]	9.4 & 21.6	9.8 & 8.1	-	≥ 9	$1.43 \times 1.43 \times 0.07$	2	Stacked patch & slotting & shorted vias
[4]	14.8 & 38.4 & 5.3	4.9 & 5.9 & 4.95	-	-	$0.73 \times 0.73 \times 0.21$	3	Defected ground structure & stubs
[5]	40 & 62	4.6 & 5.2	-	≥ 15	$0.49 \times 0.49 \times 0.35$	2	Dual antenna
[10]	4.2 & 3.9 & 3.4	7.15 & 6.02 & 4.38	-	≥ 30	-	3	Slotting & stubs
[11]	5 & 2.1 & 9.5	7.5 & 8.7 & 8.7	-	≥ 20	$0.76 \times 0.76 \times 0.03$	3	Slotting & stubs
[12]	1.2 & 2 & 1.9 & 0.9	4.6 & 5.05 5.8 & 6.3	-	≥ 30	$0.77 \times 0.77 \times 0.04$	4	Coupled resonators network
[18]	0.8 & 0.7 & 0.8 & 0.7	2.4 & 1.4 & 2 & 2.4	≥ 42	≥ 15	$0.4 \times 0.4 \times 0.02$	4	Shorting & slotting
This work	1.1 & 6.7 & 9.8	6.35 & 6.15 & 9.42	≥ 85.6	≥ 20	$0.57 \times 0.57 \times 0.02$	3	Off-centerfeeding & stacked patch

IMBW represents impedance bandwidth; PG represents peak gain; Effi represents efficiency; XPR represents cross-polarization ratio; λ_0 represents the wavelength of low frequency.

Compared with existing antennas, this paper utilizes off-center feeding technology to achieve the characteristics of tri-band resonance on a single-layer patch. The introduction of the circular parasitic patch not only widens the impedance bandwidth, but also improves the gain of the antenna. Benefiting from the diverse current distribution of the two patches, the antenna has directional and omnidirectional diverse radiation patterns. The measured results show that the radiation efficiency of higher than 85.6% and the maximum gain of greater than 9.42 dBi are obtained in a stacked structure. The impedance bandwidth of the antenna designed in this paper at f_1 and f_2 is too narrow. In conclusion, the design method in this paper is simple, easy to implement, and simultaneously obtains high gain, enhanced bandwidth, and pattern diversity on a single antenna.

5. Conclusions

A novel tri-band circular patch antenna is designed in this study by combining the technology of an off-center probe and a parasitic patch. Three resonant modes of TM_{01} , TM_{02} , and TM_{03} are achieved and attributed to the coupling effect between the stacked patches; the resonance bandwidth of the proposed antenna is broadened. Specifically, the antenna provides bandwidths of 20 MHz, 260 MHz, and 510 MHz, and antenna gains of up to 6.35 dBi, 6.15 dBi, and 9.42 dBi at f_1 , f_2 , and f_3 , respectively. Moreover, the

measured results show that differentiated radiation patterns exhibiting broadside radiation, omnidirectional radiation, and three-beam radiation in the three bands are also obtained. Compared with the multiple-band antennas proposed in [10,11,18], the antenna designed in this paper has a radiation efficiency of no less than 85% and a simple structure, which suggests that it can be applied to the multi-service field of wireless communication, such as indoor routing, with a stronger penetration ability.

Author Contributions: Theoretical analysis and modeling simulation, M.G. and X.Z.; data collection and processing, M.G. and X.Z.; funding acquisition, M.G. and X.Z.; writing—original draft, M.G. and X.Z.; writing—review and checking, X.Z. All authors have read and agreed to the published version of the manuscript.

Funding: This work was supported by the Fundamental Research Funds for the Central Universities under Grant No. 2020ZDPY0223; the Natural Science Research Funds Project of Hefei Technology College under Grant No. 2021KJA01; Hefei Technology College High-level Talent Introduction Funding Project No. 2021KYQDZ007; and the Science and Technology Innovation Team Funding Project of Hefei Technology College No. 2022Akjcx06.

Institutional Review Board Statement: Not applicable.

Informed Consent Statement: Not applicable.

Data Availability Statement: The data presented in this study are available within the article.

Conflicts of Interest: The authors declare no conflict of interest.

References

1. Liu, J.H.; Xue, Q.; Wong, H.; Lai, H.W. Design and analysis of a low-profile and broadband microstrip monopolar patch antenna. *IEEE Trans. Antennas Propag.* **2013**, *61*, 11–18. [[CrossRef](#)]
2. Gao, S.; Gei, L.; Zhang, D.G.; Qin, W. Low-profile dual-band stacked microstrip monopolar patch antenna for WLAN and car-to-car communications. *IEEE Access* **2018**, *6*, 69575–69581. [[CrossRef](#)]
3. Ge, L.; Gao, S.; Li, Y.J.; Qin, W.; Wang, J.P. A low-profile dual-band antenna with different polarization and radiation properties over two bands for vehicular communications. *IEEE Trans. Veh. Technol.* **2019**, *68*, 1004–1008. [[CrossRef](#)]
4. Gong, Y.J.; Yang, S.H.; Li, B.; Chen, Y.H.; Tong, F.L.; Yu, C.Y. Multi-band and high gain antenna using AMC ground characterized with four zero-phases of reflection coefficient. *IEEE Access* **2020**, *6*, 171457–171468. [[CrossRef](#)]
5. Guo, D.; He, K.; Zhang, Y.; Song, M. A multiband dual-polarized omnidirectional antenna for indoor wireless communications systems. *IEEE Antennas Wirel. Propag. Lett.* **2017**, *16*, 290–293. [[CrossRef](#)]
6. Liu, Y.; Li, X.; Yang, L.; Liu, Y. A dual-polarized dual-band antenna with omni-directional radiation patterns. *IEEE Trans. Antennas Propag.* **2017**, *65*, 4259–4262. [[CrossRef](#)]
7. Zhang, J.D.; Zhu, L.; Liu, N.W.; Wu, W. Dual-band and dual-circularly-polarized single-layer microstrip array based on multi-resonant modes. *IEEE Trans. Antennas Propag.* **2017**, *65*, 1428–1433. [[CrossRef](#)]
8. Wu, D.L.; Zhang, G.; Li, J.F.; Wu, Y.J.; Tian, X.X. A low-profile antenna with omnidirectional and unidirectional radiation patterns over two operation bands. *IEEE Access* **2019**, *7*, 182691–182700. [[CrossRef](#)]
9. Yang, X.J.; Ji, Y.; Ge, L.; Zeng, X.R.; Wu, Y.L. A dual-band radiation-differentiated patch antenna for future wireless scenes. *IEEE Antennas Wirel. Propag. Lett.* **2020**, *19*, 1007–1011. [[CrossRef](#)]
10. Qian, J.F.; Chen, F.C.; Chu, Q.X. A novel tri-band patch antenna with broadside radiation and its application to filtering antenna. *IEEE Trans. Antennas Propag.* **2018**, *66*, 5580–5585. [[CrossRef](#)]
11. Tan, Q.; Chen, F.C. Tri-band circularly polarized antenna using a single patch. *IEEE Antennas Wirel. Propag. Lett.* **2020**, *19*, 2013–2017. [[CrossRef](#)]
12. Mao, C.X.; Gao, S.; Wang, Y.; Izquierdo, B.S. A novel multi-band directional antenna for wireless communications. *IEEE Antennas Wirel. Propag. Lett.* **2017**, *16*, 1217–1220. [[CrossRef](#)]
13. An, W.X.; Wang, X.; Fu, H.P.; Ma, J.G.; Huang, X.D.; Feng, B.T. Low-profile wideband slot-loaded patch antenna with multiresonant modes. *IEEE Antennas Wirel. Propag. Lett.* **2018**, *17*, 1309–1313. [[CrossRef](#)]
14. Xu, H.X.; Wang, G.M.; Lv, Y.Y.; Qi, M.Q.; Gao, X.; Ge, S. Multifrequency monopole antennas by loading metamaterial transmission lines with dual-shunt branch circuit. *Prog. Electromagn. Res.* **2013**, *137*, 703–725. [[CrossRef](#)]
15. Xu, H.X.; Wang, G.M.; Qi, M.Q.; Cai, T. Compact fractal left-handed structures for improved cross-polarization radiation pattern. *IEEE Trans. Antennas Propag.* **2014**, *62*, 546–554. [[CrossRef](#)]
16. Xu, H.X.; Wang, G.M.; Qi, M.Q.; Zhang, C.X.; Liang, J.G.; Gong, J.Q.; Zhou, Y.C. Analysis and design of two-dimensional resonant-type composite right/left-handed transmission lines with compact gain-enhanced resonant antennas. *IEEE Trans. Antennas Propag.* **2013**, *61*, 735–747. [[CrossRef](#)]

17. Lee, K.F.; Ho, K.; Dahele, J. Circular-disk microstrip antenna with an air gap. *IEEE Trans. Antennas Propag.* **1984**, *32*, 880–884.
18. Boukarkar, A.; Lin, X.Q.; Jiang, Y.; Yu, Y.Q. Miniaturized single-feed multi-band patch antennas. *IEEE Trans. Antennas Propag.* **2017**, *65*, 850–854. [[CrossRef](#)]